Three-Dimensional Numerical Simulation of Segregation in Powder Injection Molding

Ilinca, Florin; Hétu, Jean-Francois

Publisher's version / Version de l'éditeur:
http://dx.doi.org/10.3139/217.2123
International Polymer Processing, 2, pp. 208-215, 2008

2007 - 11779_G
CNRC _ 50203

Three-Dimensional Numerical Simulation of Segregation in Powder Injection Molding

Florin Ilinca

Jean-François Hétu

Industrial Materials Institute, National Research Council,

75, de Mortagne, Boucherville, Québec, Canada, J4B 6Y4

Email: florin.ilinca@cnrc-nrc.gc.ca

Phone: (450) 641-5072

FAX: (450) 641-5106

July 24, 2007

A paper submitted for publication in the **International Polymer Processing** Journal

All correspondence to be sent to: Dr. F. Ilinca.

Abstract

The ability to predict segregation of the solid phase in processes such as powder injection molding and injection molding of semi-solid materials is of special interest since such phenomenon affects the final properties and characteristics of the molded parts. In powder injection molding, for example, defects appear very often in the debinding and sintering stages but are caused by filling problems and determined by a non-uniform distribution of the solid particles within the molded part. In this paper we propose a 3D numerical solution algorithm for the simulation of particle migration in dense suspensions. The particle migration is modeled using the diffusion flux model and integrated into the NRC's 3D injection molding software. The solution algorithm is validated by solving flow problems for which experimental and numerical data are available: circular Couette flow, piston driven flow and sudden contraction-expansion flow. Since it is observed that the piston movement in the sleeve can induce particle migration even before the material enters the cavity, an ALE (Arbitrary Lagrangian-Eulerian) formulation is also developed to include the piston movement in molding simulations. The ALE formulation is first compared with an Eulerian solution for the case of the piston driven flow problem. Then, the approach is applied to injection molding problems and the segregation inside the molded parts is studied.

Keywords: Powder Injection Molding, 3D Modeling, Finite Elements, Segregation, Diffusive flux model.

1. INTRODUCTION

Segregation of the solid phase in powder injection molding (PIM) is of special interest since it affects the final properties and characteristics of the molded parts. PIM defects appear very often in the debinding and sintering stages but are often caused by filling problems and determined by

a non-uniform distribution of the solid particles within the solution. Inhomogeneous particle distribution affects the apparent viscosity and thus the flow during filling. This distribution may also affect the part deformation during sintering and consequently the final part geometry.

Various models have been proposed to describe the separation of the solid and fluid constituents in dense suspensions. In mixture models each constituent is considered as distinct specie of a mixture. The development of the mixture formulation is done by writing the conservation equations for each phase involved in the system. Two sets of momentum, mass and energy conservation equations are therefore written, one set for the liquid phase and one for the solid phase. These coupled equations can be solved directly [1,2]; however, for computational efficiency reasons, it is usually further simplified using phase mixture rules. By doing so, the two sets of conservation equations are reduced to one set of conservation equations into which the unknowns are the average mixture velocity, pressure and temperature; the local concentration of the mixture is computed using an additional phase concentration equation [3,4].

PIM can also be modeled using dense suspension models. Dense suspension models have been developed to predict shear induced particle segregation. Conceptually, such models assume that particle-particle collision occurring in the suspension is the main driving force for phase separation. High-shear regions have a higher collision probability than low shear regions, thus based on probabilistic arguments, particles tends to migrate from the high shear flow regions to the low shear flow regions. Phillips *et al.* [5] introduced the diffusive flux model based on the concept of particle concentration diffusion. Experimental validation of the model for simple one- or two-dimensional problems is shown in Refs. [6,7]. The suspension balance model was first introduced by Nott and Brady [8] who introduced the concept of suspension 'temperature'. Morris and Boulay [9] modified the model to take into account the effect of the normal stress difference, whereas Fang et al. [10] used a flow aligned tensor to model the normal stress

difference for both diffusive flux model and suspension balance model. Experimental validation of both diffusive flux and suspension balance models is shown in Refs. [11,12].

In this paper we propose a 3D numerical solution algorithm for the simulation of particle migration in dense suspensions. The particle migration is modeled using the diffusion flux model proposed by Phillips et al. [5]. The particle migration model is integrated into the NRC's 3D injection molding software [13]. The solution algorithm is validated by solving flow problems for which experimental and numerical data are available: circular Couette flow, piston driven flow and sudden contraction-expansion flow [6,10]. An ALE formulation is also developed to treat the piston movement in injection molding problems. The ALE formulation is first compared with an Eulerian solution for the case of the piston driven flow problem. Then the approach is applied to injection molding problems and the segregation inside the molded parts is studied.

2. MODEL EQUATIONS

2.1. Flow equations

The flow of incompressible fluids is described by the Navier-Stokes equations

$$\rho\left(\frac{\partial \mathbf{u}}{\partial t}+\mathbf{u}_c\cdot\nabla\mathbf{u}\right)=-\nabla p+\nabla\cdot(2\eta D_{ij}), \tag{1}$$

$$-\nabla\cdot\mathbf{u}=0, \tag{2}$$

where η is the apparent viscosity of the suspension and $D_{ij}=(\nabla\mathbf{u}+(\nabla\mathbf{u})^T)/2$ is the strain rate tensor.

Heat transfer is modeled by the energy equation:

$$\rho c_p\left(\frac{\partial T}{\partial t}+\mathbf{u}_c\cdot\nabla T\right)=\nabla\cdot(k\nabla T)+2\eta D_{ij}D_{ij}. \tag{3}$$

In the above equations, t, $\mathbf{u}$, p, T, ρ, η, c_p and k denote time, velocity, pressure, temperature, density, viscosity, specific heat and thermal conductivity respectively. The convection velocity $\mathbf{u}_c$ is equal to the fluid velocity $\mathbf{u}$ in an Eulerian frame of reference, but depends on the mesh velocity $\mathbf{u}_m$ in an ALE formulation:

$$\mathbf{u}_c = \mathbf{u} - \mathbf{u}_m \tag{4}$$

The viscosity of the mixture is considered function of the solid fraction as given by

$$\eta = \eta_r \eta_s, \ \eta_r = \left(1 - \bar{\phi}\right)^{-1.82}, \tag{5}$$

where η_s is the viscosity of the suspension (liquid phase), η_r is the relative viscosity of the mixture with respect to that of the suspension, and $\bar{\phi}$ denotes the normalized solid fraction, $\bar{\phi} = \phi / \phi_m$. Here ϕ denotes the solid fraction and ϕ_m its maximum value (ϕ_m=0.68 for the present work).

2.2. Phase segregation

The segregation of solid particles is modeled by the diffusive flux model of Phillips et al. [5]. The solid fraction is therefore obtained by solving the transient advective-diffusive equation

$$\frac{\partial \phi}{\partial t} + \mathbf{u}_c \cdot \nabla \phi = -\nabla \cdot \mathbf{N} \tag{6}$$

where the diffusive flux $\mathbf{N}$ is given by

$$\mathbf{N} = \mathbf{N}_c + \mathbf{N}_\eta, \tag{7}$$

with $\mathbf{N}_c$ describing the interaction caused by varying collision frequency and $\mathbf{N}_\eta$ describing the interaction caused by spatially varying viscosity:

$$\mathbf{N}_c = -a^2 \phi K_c \nabla \left(\dot{\gamma} \phi\right), \tag{8}$$

$$\mathbf{N}_\eta = -a^2\phi^2\dot{\gamma}K_\eta\nabla(\ln\eta). \tag{9}$$

In the above equations a represents the radius of solid particles in the suspension, $\dot{\gamma} = \sqrt{2D_{ij}D_{ij}}$ is the shear rate, and K_c, K_η are model constants. In the standard form proposed by Phillips et al. [5] they take on the values K_c=0.41, K_η=0.62.

2.3. Mold filling simulation

For mold filling applications, in addition to the momentum-mass and energy conservation equations we have to solve for the free surface. In this work the position of the flow front is determined using a pseudo-concentration method [14]. A smooth function $F(\mathbf{x},t)$ such that the critical value, F_c, represents the position of the interface. A value larger than F_c indicates a filled region. The pseudo-concentration function is transported using the convection velocity provided by the solution of the momentum-continuity equations:

$$\frac{\partial F}{\partial t} + \mathbf{u}_c \cdot \nabla F = 0 \tag{10}$$

2.4. ALE formulation

In most injection molding applications the material is pushed into the mold cavity by means of a plunger. As shown later in the piston driven flow application, to represent the flow behavior and segregation mechanism we need to model the plunger advancement and hence consider changes in the computational domain. This is done by means of an Arbitrary Lagrangian-Eulerian formulation (ALE) with the geometrical change given by simple relationships depending on the plunger speed. The change of the computational domain in time is illustrated in Figure 1. The portion of the computational domain located between the initial plunger position $x=x_i$ and a fixed location $x=x_0$ changes in time to account for the actual plunger position. At any given time t, this

volume will be considered between the actual plunger location $x=x_i+v_pt$ and the fixed location $x=x_0$. The mesh is therefore deformed in time as given by the change of variables $x \rightarrow x^*$:

$$x^* = x + \frac{x_0 - x}{x_0 - x_i} u_p t \qquad \text{for} \qquad x \in [x_i, x_0] \tag{11}$$

where u_p is the plunger velocity, x is the coordinate of a mesh point in the initial un-deformed mesh (at $t=0$) and x^* is the coordinate of the respective point in the deformed mesh. At the end of the filling ($t=t_f$) the plunger will be located at $x=x_f$ where $x_f=x_i+u_pt_f$. As the mesh deforms, the ALE formulation of the conservation equations has to take into account for the mesh velocity given by:

$$\begin{aligned} u_m &= \frac{x_0 - x}{x_0 - x_i} u_p \qquad \text{for} \qquad x \in [x_i, x_0] \\ u_m &= 0 \qquad\qquad\quad \text{for} \qquad x \notin [x_i, x_0] \end{aligned} \tag{12}$$

The convection velocity is then computed using Eq. (4).

2.5. Boundary conditions

A combination of Dirichlet and Neuman boundary conditions is imposed for velocity, pressure, temperature, front tracking function and solid fraction. For injection molding applications, no-slip boundary conditions are imposed on the cavity walls filled by the polymer, while on the unfilled part, a free boundary condition allows for the formation of the typical fountain flow. The heat transfer between the cavity and the mold is given by

$$q_m = h_c(T - T_m) \qquad \text{on} \quad \Gamma_{\text{mold}}, \tag{13}$$

where h_c is a surface heat transfer coefficient and T_m is the mold temperature. The solid fraction is set to an initial value and then a zero solid fraction flux is imposed on the boundary. This will ensure that there is no flux of solid particles across the boundary of the computational domain.

3. FINITE ELEMENT SOLUTION

Model equations are discretized in time using a first order implicit Euler scheme. Linear continuous interpolation functions are used for all variables. At each time step, the global system of equations is solved in a partly segregated manner: momentum-continuity ($\mathbf{u}$,p), energy (T), solid phase concentration, and then the front tracking equation. The incompressible Navier-Stokes equations (1), (2) are solved using a Galerkin Least-Squares method [15], the energy equation is solved by a combined SUPG/GGLS (Streamline Upwind Petrov-Galerkin / Galerkin Gradient Least-Squares) method [15], and the front tracking equation is discretized by a SUPG method. A SUPG method is also used for the solution of the solid phase concentration. The finite element formulation for the solid fraction equation is as follows:

$$\begin{aligned} &\int_{\Omega}\left(\frac{\partial \phi}{\partial t}+\mathbf{u}_c\cdot\nabla\phi\right)w d\Omega-\int_{\Omega}\left(\mathbf{N}_c+\mathbf{N}_\eta\right)\cdot\nabla w d\Omega+ \\ &\sum_K\int_{\Omega_K}\left(\frac{\partial \phi}{\partial t}+\mathbf{u}_c\cdot\nabla\phi\right)\tau\mathbf{u}_c\cdot\nabla w d\Omega_K=-\int_{\partial\Omega}\left(\mathbf{N}_c+\mathbf{N}_\eta\right)\cdot\hat{\mathbf{n}} w d\Gamma. \end{aligned} \tag{14}$$

The integrals in the first row together with the right hand side term represent the standard Galerkin formulation with the diffusive flux integrated by parts. Integrals over the element interiors represent the stabilization terms. The flux of particles across the boundary is zero and therefore the boundary integral in the right hand-side of (14) vanishes.

4. VALIDATION

In this section the solution algorithm is validated on cases for which both experimental and numerical data are available: circular Couette flow, piston driven flow and sudden contraction-expansion flow [6,10].

4.1. Circular Couette Flow

This application was the object of an experimental study by Abbott et al. [16] and reinvestigated both numerically and experimentally by Tetlow et al. [7]. The experimental apparatus has the inner rod (R_i) of 0.64 cm and the inner radius of the outer tube (R_o) of 2.38 cm. The particle radius a is 675 μm.

The flow is axi-symmetric and can be solved using the model equations written in cylindrical coordinates. Because the variables depend only along the tube radius a simplified one-dimensional problem can be obtained. The only variables to be solved are the circumferential velocity v_θ and the solid fraction ϕ, as the axial and radial velocity components are zero, whereas the pressure is constant. The 1D problem for the circular Couette flow writes as:

$$\frac{1}{r^2}\frac{\partial}{\partial r}\left[\eta r^3 \frac{\partial}{\partial r}\left(\frac{v_\theta}{r}\right)\right]=0 \tag{15}$$

$$\frac{\partial \phi}{\partial t}=\frac{1}{r}\frac{\partial}{\partial r}\left[ra^2\phi K_c \frac{\partial}{\partial r}(\dot{\gamma}\phi)\right]+\frac{1}{r}\frac{\partial}{\partial r}\left[ra^2\phi^2\dot{\gamma}K_\eta \frac{\partial}{\partial r}(\ln\eta)\right] \tag{16}$$

The problem is solved using both the 3D solution algorithm and the 1D model equations. This way the 3D algorithm is validated using the 1D solution as a reference. Then the predictive capability of the model is quantified by comparing the numerical results with the experimental data.

The initial particle concentration ϕ_0 is taken constant. The numerical solution is first compared with the experiment during the transient evolution in Figure 2. For this case the particles diameter is 655μm, the initial solid fraction is 0.5 and the inner rod rotates at 17rpm. As can be seen, the 1D and 3D solutions are almost identical and the model prediction agrees well with experimental observation. The velocity at steady state for the same conditions is compared with the measured

one in Figure 3. The Newtonian velocity profile is also shown for comparison purposes. Here again the numerical solutions agree well with the data indicating that the viscosity model is appropriate.

The steady-state particle distribution for various initial solid fractions is shown in Figure 4. Only the 3D solution is compared with the experiment here. For these cases the particles diameter is 675μm and the inner rod rotates at 17rpm. Observe however, that at steady-state both the transient and convective terms vanish (the velocity is normal to the solid fraction gradient) and the solution does not depend on the particle size but only on the initial value of the particle concentration. The numerical results are in good agreement with the experimental data of Abbott et al. [16] and are similar with those reported by Fang et al. [10]. In Figure 5 the 1D and 3D solutions are compared for different mesh density and for an initial solid fraction of 0.5. As can be seen, the two solution methods results in similar results and the effect of the mesh size is negligible. The only discrepancy is observed for the solution on the coarser mesh at the inner rod surface and is explained by the fact that in the 1D case the derivative of the shear rate at the boundary is more accurate than the one used in the 3D solution.

4.2. Piston driven flow

This test case consists of displacing a fixed volume of suspension down a pipe by means of a piston. The material exhibits a similar behavior in injection molding where the suspension is pushed by a piston and forms a free surface. The uniformity of the suspension downstream of the piston will then affect the distribution of particles inside the molded part. An experimental study of this problem was performed by Subia et al. [6]. The piston radius is 2.54 cm and the pipe was filled with material on a length of 30 cm. The suspension contained 50% of spherical particles having 3178 μm in diameter. The piston moves from left to right at a speed of 0.0625 cm/s, while

the pipe was held stationary. A first computation was carried out on a fixed mesh by considering that the pipe moved from right to left and the pistons were maintained fixed. The flow pattern after the piston was displaced with 15 piston diameters is shown in Figure 6. Segregation of solid particles for different positions of the piston is shown in Figure 7. The solid fraction decreases in front of the piston that pushes the suspension and is higher in the second half of the domain along the pipe axis. This is in agreement with experimental observation [6].

The mean solid fraction on sections normal to the pipe axis was computed and plotted along the pipe axis in Figure 8. The results are compared with experimental data collected after the piston was displaced with 5 piston diameters. The numerical solution recovers correctly the segregation behavior, but slightly underestimates the change in the solid fraction. Simulation indicates that segregation in front of a moving piston produces quite rapidly and that a somehow steady distribution is attained after a 10D piston displacement.

This problem describes well the behavior of the material during injection molding. However, simulation of the piston movement in material processing would not be possible in an Eulerian frame of reference, since the model includes both the moving piston and stationary parts as the mold cavity. Therefore the more general Arbitrary Lagrangian Eulerian (ALE) formulation described in Section 2.4 needs to be considered. Results using the ALE formulation for the piston driven flow with a free surface on the right hand-side are shown in Figures 9 and 10. The ALE results are very close to those given by the Eulerian approach (Figures 7 and 8). Small differences are observed on the right hand-side of the computational domain, where a non-planar free surface is present in the ALE solution and a flat no-slip surface is present in the Eulerian case. This test case indicates that the ALE approach performs well and can be used for injection molding applications.

4.3. Sudden contraction-expansion flow

This test case was the subject of an experimental study by Altobelli et al. [17]. The suspension is pushed by a piston from a reservoir pipe into a smaller diameter pipe and then into another larger catch pipe. The reservoir pipe and the catch pipe have a diameter of 5.08 cm, while the smaller pipe has an inner diameter of 1.27 cm. The smaller diameter pipe is 38 cm long. Initially 30 cm of the reservoir pipe, the entire smaller diameter pipe and 4 cm of the catch pipe were filled. The plunger was displaced at a constant velocity of 0.0625 cm/s, resulting in a mean velocity of 1 cm/s in the smaller pipe. The solid particles in the suspension were 50% by volume with a mean particle diameter of 675 μm.

The numerical solution was obtained using the ALE formulation. The computational mesh and solid fraction after the piston moves 2, 4 and respective 6 larger section diameters are shown in Figure 11. The mean solid fraction along the pipe axis is shown in Figure 12. Several observations can be drawn from these results. First we remark that the solid fraction decreases at the surface of the moving piston, observation made also in the case of the piston driven flow. Second we observe a sharp increase in the solid fraction just prior to the 4:1 contraction (x=0cm). The solid fraction decreases then rapidly and reaches smaller values along the smaller diameter pipe. Third, we remark that at the 1:4 expansion, x=38cm, the solid fraction decreases before the section change and increases on a very small region after the expansion. In the catch pipe, x>38cm, the solid fraction is initially smaller than the mean value of 0.5, but increases towards the end of the pipe.

Figure 13 shows the solid fraction distribution in radial direction at various locations along the smaller diameter pipe together with the experimental data of Altobelli et al. [17]. Results are plotted for x/L=0.1, 0.5 and 0.95, where L denotes the length of the smaller diameter pipe and x is

the coordinate along the pipe measured in the sense of the flow (from the contraction, x=0, towards the expansion, x=L). The results indicate that the solid fraction is larger near the axis of the pipe and decreases close to the pipe wall. We remark also that the segregation is more pronounced at x/L=0.5 and 0.95 than at the entry of the smaller diameter pipe. These observations agree well with the experimental findings of Altobelli et al. [17].

5. MOLD FILLING APPLICATION

In this application the ALE formulation is used to solve the injection molding of a rectangular plate. The plate is 8 cm by 6 cm and has 4 mm in thickness. The filling piston has a radius of 1 cm and his displacement is 13.2 cm. Filling of the plate is made through a circular gate with a radius of 2 mm. The suspension contains particles of 50 μm in radius and the initial solid fraction is uniform at 50%. Complete filling of the plate takes 10 s. The filling pattern and the solid fraction distribution is shown in Figure 14 after 1.8 s, 4 s, 7.2 s and respectively 10 s. The figure shows a cut along the symmetry plane parallel to the longest side of the plate in order to see the solid fraction distribution inside the part. The images show both the complete domain (where the displacement of the piston during the filling is clearly seen) and details of the flow inside the plate. Segregation of solid particles is apparent inside the pipe as previously observed for the piston driven flow case. This causes the material to enter the gate with a non-uniform solid fraction. Additional segregation is observed inside the gate where shear rates are highest. Finally, the molded part has higher solid fraction in the mid-plane and on the outside boundaries of the plate and lower solid fraction on the upper and lower surfaces.

6. CONCLUSION

In this paper a three-dimensional finite element algorithm is shown for the solution of the flow of dense suspensions. The segregation of solid particles is described by a diffusive flux model. Validations cases show a good agreement with experimental data and previously published numerical solutions. The application to injection molding problems is done by using an ALE formulation. For the piston driven flow the ALE formulation is shown to provide similar results as an Eulerian approach on a fixed mesh, thus indicating that the procedure performs well. Application to the mold filling of a rectangular plate shows the ability to use this method to the solution of powder injection molding.

REFERENCES

1. T. Barrière, J.C. Gelin and B. Liu, *J. of Material Process. Techn., A*, **125-126**:518-524 (2002).
2. J. Petera and M. Kotynia, *Int. J. Heat Mass Transfer*, **47**:1483-1498, (2004).
3. M. Manninen and V. Taivassalo, On the mixture model for multiphase flow, *VTT Publications 288*, Finland (1996).
4. F. Pineau, F. Ilinca and J.-F. Hétu, A mixture approach for semisolid metal mold filling simulations, *Proc. MCWASP 2006*, TMS (2006).
5. R.J. Phillips, R.C. Armstrong, R.A. Brown, A.L. Graham and J.R. Abott, *Physics of Fluids, A*, **4**:30-40 (1992).
6. S.R. Subia, M.S. Ingber, L.A. Mondy, S.A. Altobelli and A.L. Graham, *Journal of Fluid Mechanics*, **373**:193-219 (1998).
7. N. Tetlow, A.L. Graham, M.S. Ingber, S.R. Subia, L.A. Mondy and S.A. Altobelli, *J. Rheol.*, **42**(2):307-327 (1998).

8. P. R. Nott and J.F. Brady, *J. Fluid Mech.*, **275**:157-199 (1994).

9. J.F. Morris and F. Boulay F., *J. Rheol.*, **43**(5):1213-1237 (1999).

10. Z. Fang, A.A. Mammoli, J.F. Brady, M.S. Ingber, L.A. Mondy and A.L. Graham, *Int. J. of Multiphase Flow*, **28**:137-166 (2002).

11. M.K. Lyon and L.G. Leal, *J. Fluid Mech.*, **363**:25-56 (1998).

12. N.C. Shapley, R.A. Brown and R.C. Armstrong, *J. Rheol.*, **48**(2):255-279 (2004).

13. F. Ilinca and J.-F. Hétu, *Int. Polym. Proc.*, **16**, 291 (2001).

14. F. Ilinca and J.-F. Hétu, *Int. J. Num. Methods Fluids,* **34**, 729-750 (2000).

15. F. Ilinca and J.-F. Hétu, *Int. J. Num. Methods Fluids,* **50**, 1445-1460 (2006).

16. J.R. Abbott, N. Tetlow, A.L. Graham, S.A. Altobelli, E. Fukushima, L.A. Mondy and T.S. Stephens, *J. Rheol.*, **35**(5):773-795 (1991).

17. S.A. Altobelli, E. Fukushima and L.A. Mondy, *J. Rheol.*, **41**(5):1105-1115 (1997).

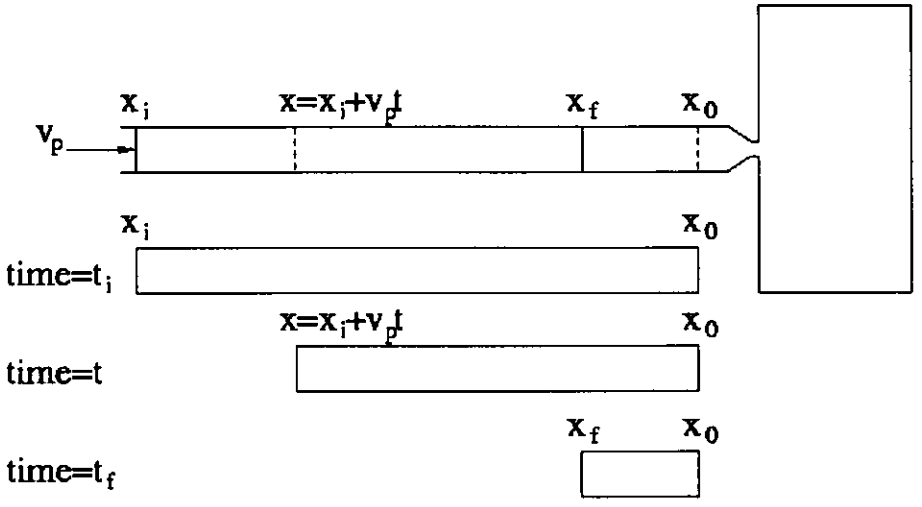

FIGURE 1. Computational domain changes from plunger movement.

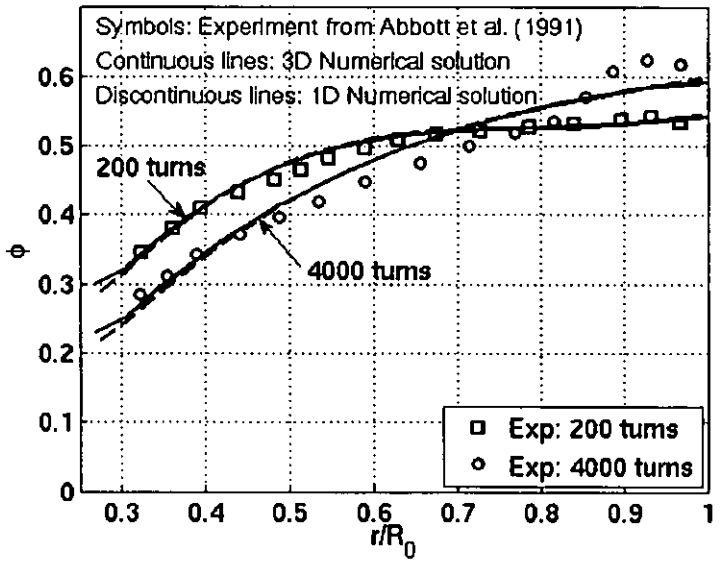

FIGURE 2. Transient Couette flow: Comparison of numerical predictions with experimental data of Abbott et al. [16].

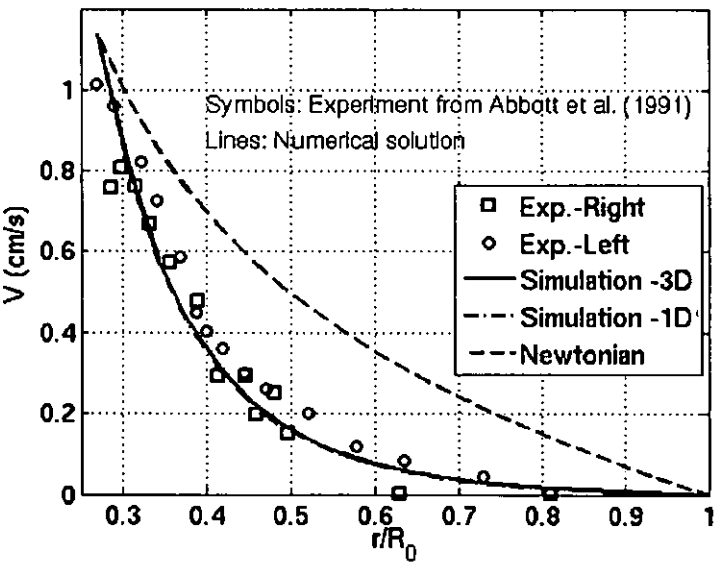

FIGURE 3. Circular Couette flow: Comparison of predicted velocity profile with experimental data of Abbott et al. [16].

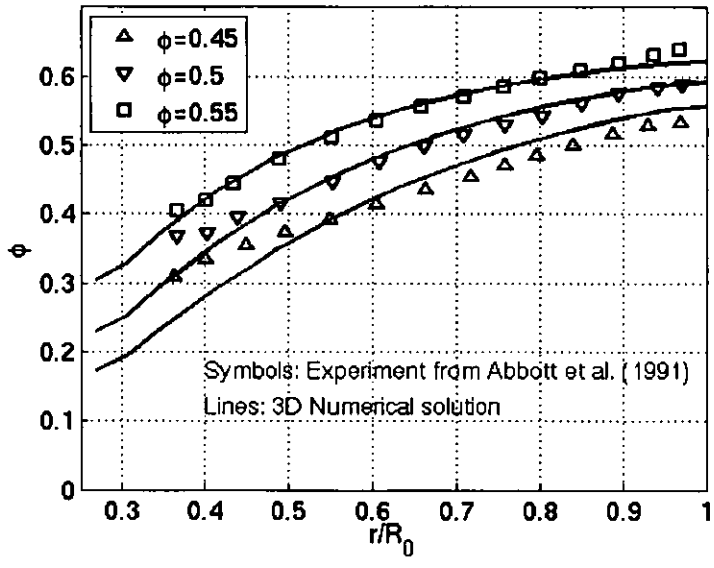

FIGURE 4. Comparison of model prediction with experimental particle concentration profiles of Abbott et al. [16].

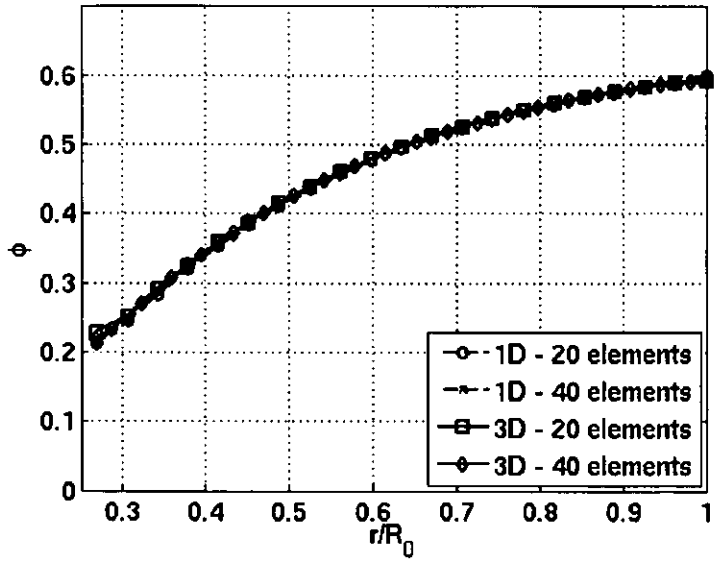

FIGURE 5. Circular Couette flow: Effect of mesh size on the 1D and 3D solutions for ϕ_0=0.5.

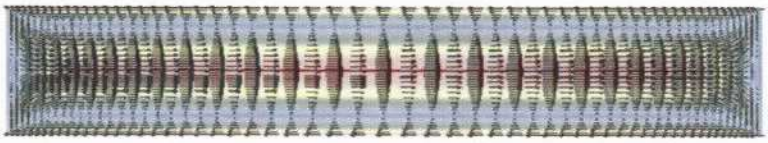

FIGURE 6. Velocity distribution for piston driven flow after 15 piston diameters (15D) for Eulerian approach.

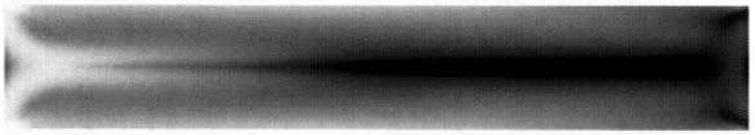

(a) After 5D

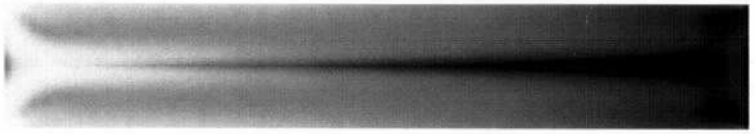

(b) After 10D

(c) After 15D

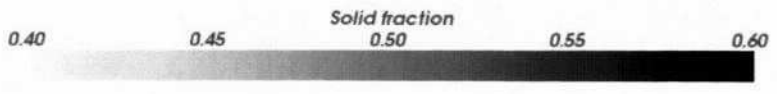

FIGURE 7. Distribution of solid fraction for various piston displacements (Eulerian approach).

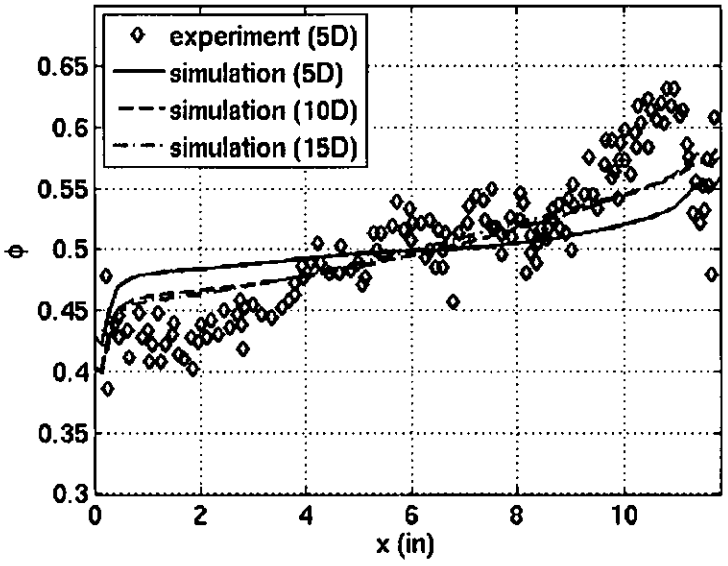

FIGURE 8. Mean solid fraction along the tube axis using an Eulerian approach (experimental data from Subia et al. [6]).

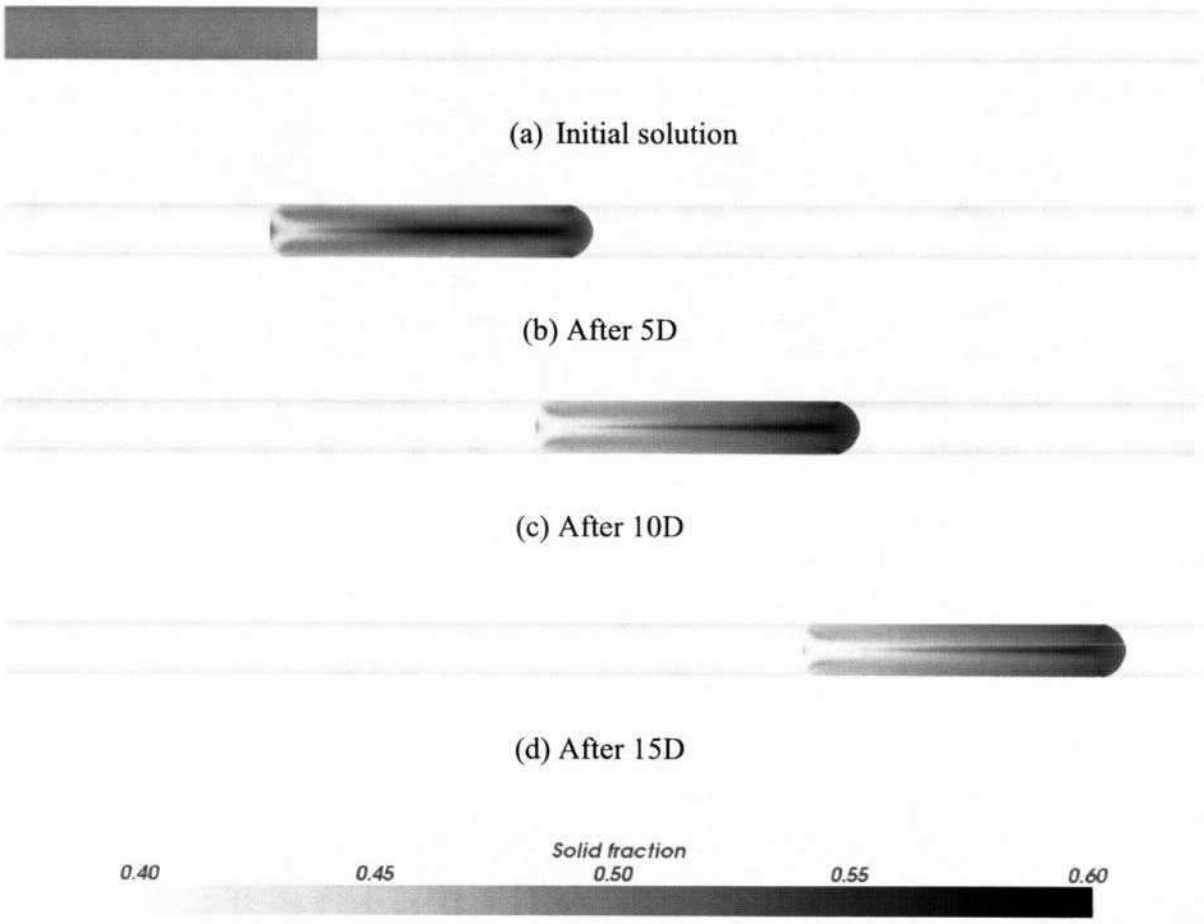

FIGURE 9. Distribution of solid fraction for various piston displacements (ALE approach).

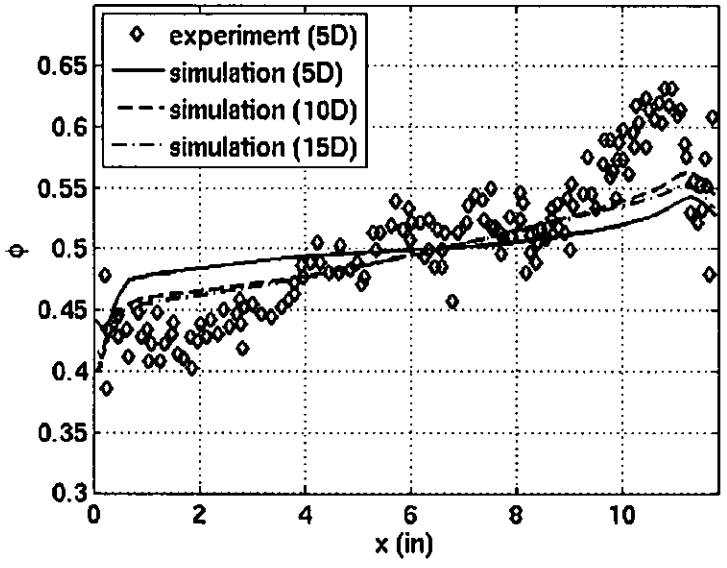

FIGURE 10. Mean solid fraction along the tube axis using an ALE approach (experimental data from Subia et al. [6]).

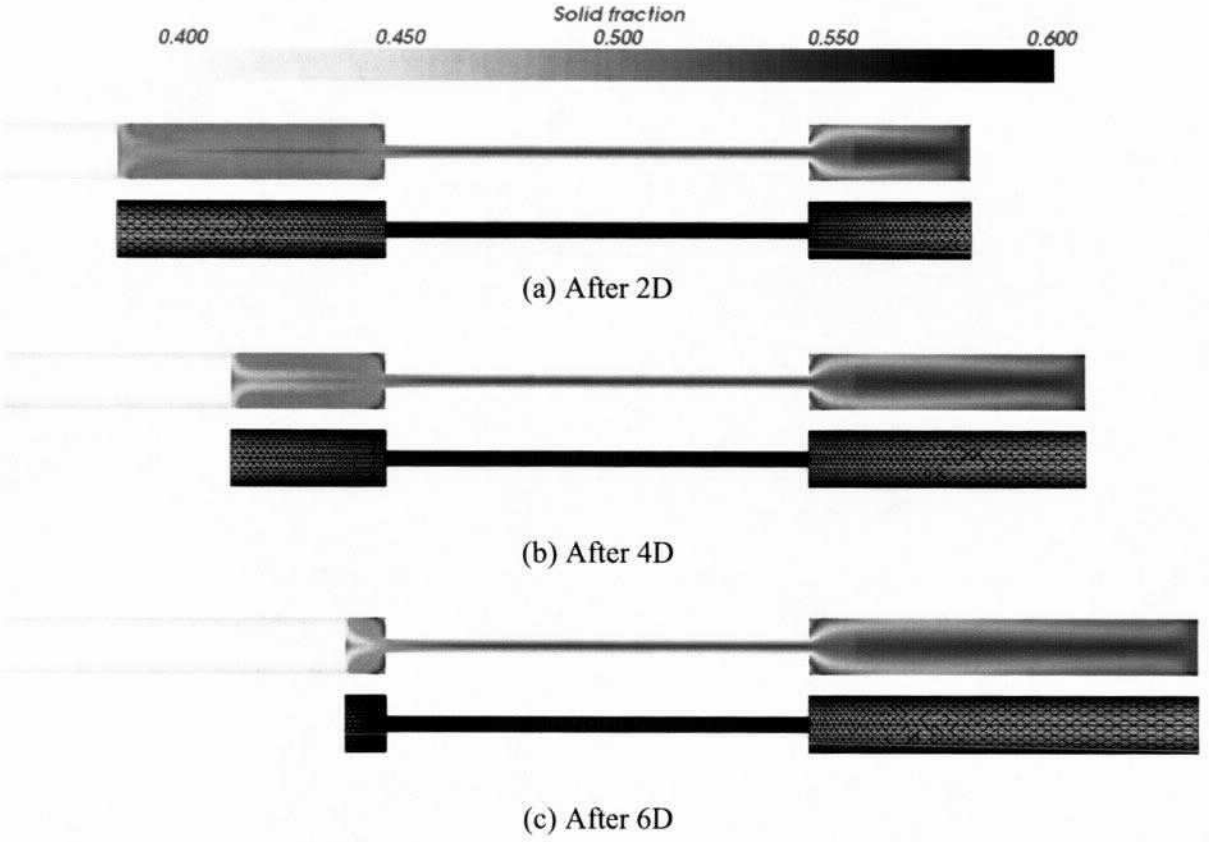

(a) After 2D

(b) After 4D

(c) After 6D

FIGURE 11. Contraction-expansion flow: Distribution of solid fraction and computational mesh for various piston displacements.

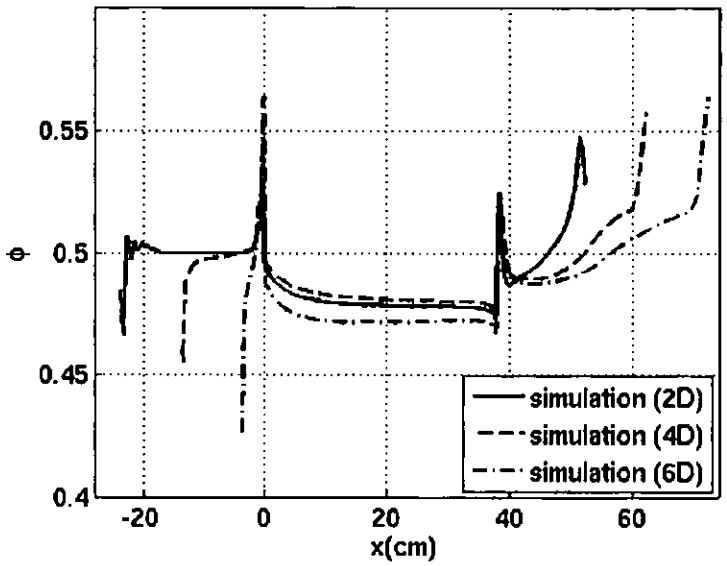

FIGURE 12. Sudden contraction-expansion flow: Mean solid fraction along the pipe axis.

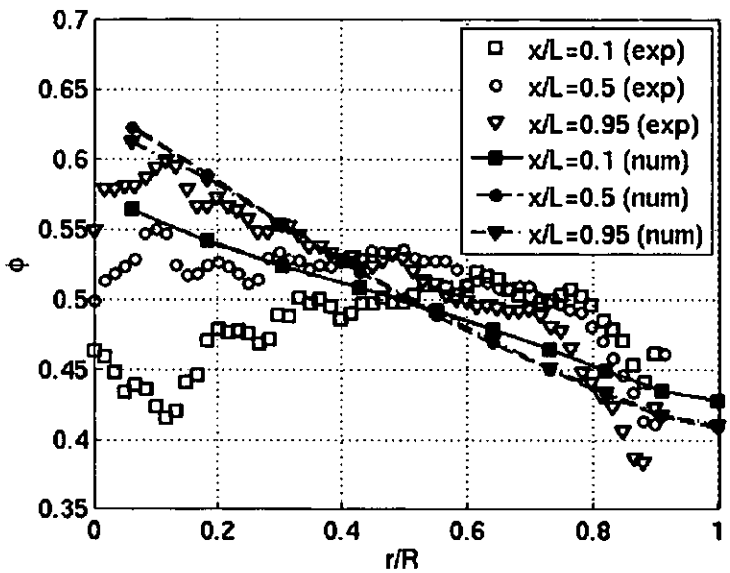

FIGURE 13. Solid fraction in radial direction at various locations along the smaller diameter pipe.

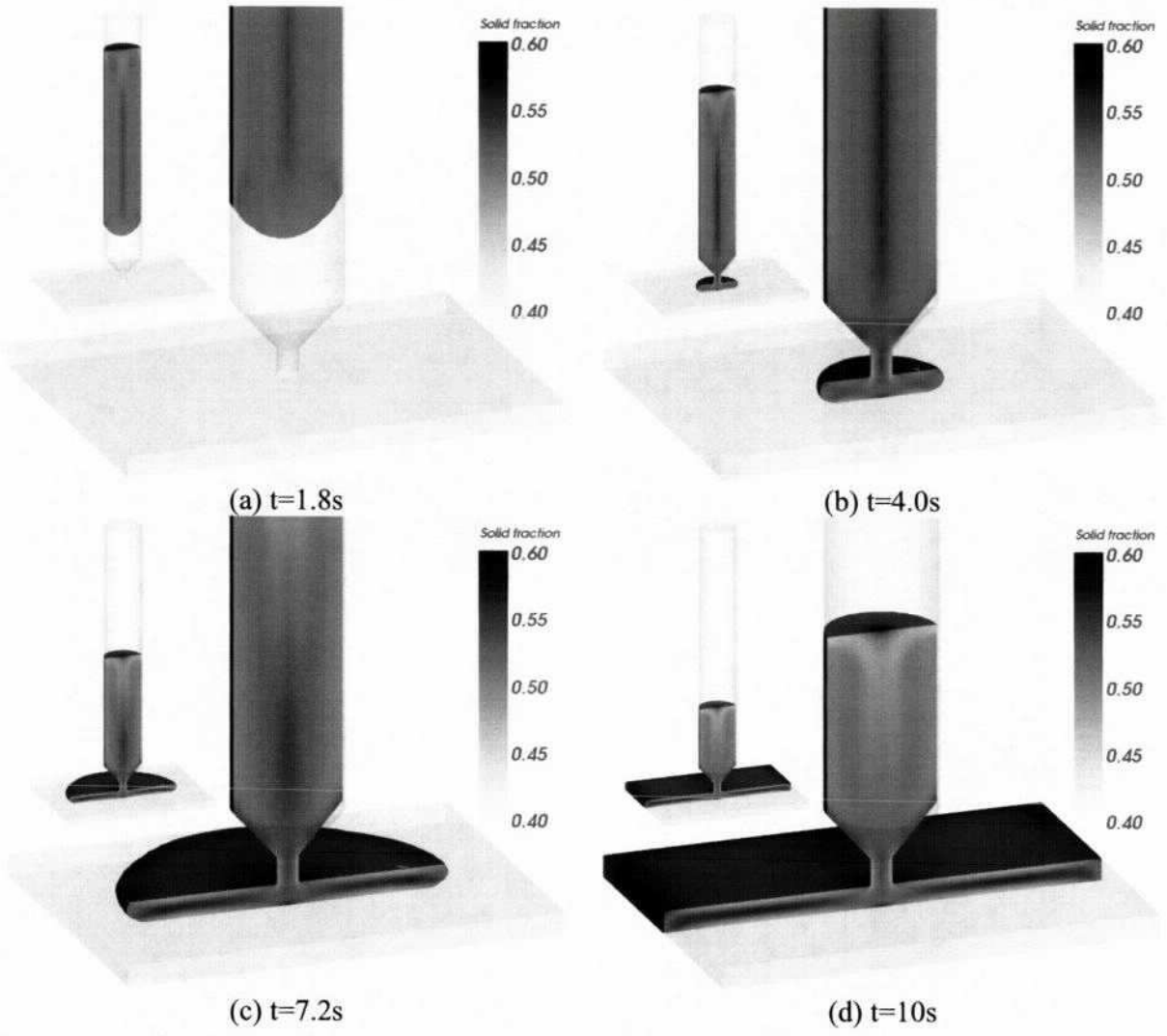

FIGURE 14. Distribution of solid fraction for the injection of a plate.